Applied Surface Science 360 (2016) 1016–1022

Contents lists available at ScienceDirect

Applied Surface Science

journal homepage: www.elsevier.com/locate/apsusc

Boron doped g-C_3N_4 with enhanced photocatalytic UO_2^{2+} reduction performance

Changhai Lu[a], Rongyue Chen[a], Xi Wu[a], Meifeng Fan[a], Yunhai Liu[a], Zhanggao Le[a], Shujuan Jiang[a,*], Shaoqing Song[a,b,*]

[a] Key Laboratory for Radioactive Geology and Exploration Technology, Fundamental Science for National Defense, East China University of Technology, Nanchang 330013, PR China
[b] State Key Laboratory of Advanced Technology for Material Synthesis and Processing, Wuhan University of Technology, Wuhan 430070, PR China

ARTICLE INFO

Article history:
Received 11 September 2015
Received in revised form
10 November 2015
Accepted 11 November 2015
Available online 25 November 2015

Keywords:
Graphitic carbon nitride
Boron doping
Photocatalysis
UO_2^{2+} reduction

ABSTRACT

Tuning the band gap and absorption intensity of visible-light by element doping is an attractive strategy to enhance the photocatalytic activity of semiconductor materials. Here we doped boron into g-C_3N_4 to construct highly efficient photocatalysts (B-g-C_3N_4) for the photocatalytic reduction of UO_2^{2+}. Characterization and photocatalysis tests showed the band gap of B-g-C_3N_4 was narrowed, and the absorption intensity of visible-light was enhanced with increasing the formed N-B-C (B_{CN}) of B-g-C_3N_4, which is consistent with the trend of the photocatalytic performance of B-g-C_3N_4. The optimized B-g-C_3N_4 photocatalyst with B_{CN} content of 1.01 at.% exhibited excellent removal efficiency of UO_2^{2+} and good photocatalytic stability. Therefore, these results may lead to a new strategy for exploring the advanced photocatalysts based on the carbon nanomaterials with abundant B_{CN} for the photocatalytic reduction of U(VI) pollutant.

1. Introduction

With the rapid development of nuclear industry, radioactive pollution has become one of the most complex environmental problems [1,2]. Uranium is a typical radioactive pollutant released from uranium mining, nuclear research, fuel production, and weapons manufacturing. A long-term exposure to uranium can cause serious health problems such as severe liver damage, kidney damage, and eventual death [3]. Therefore, the elimination of the uranium species exposed on environment is an important issue. Study reports show that uranium species can exist in several oxidation states (e.g., U(0), U(III), U(IV), and U(VI)), in which the predominant oxidation states in the ambient environment are soluble U(VI) and slightly soluble U(IV) [4,5]. Reduction of soluble U(VI) to insoluble uranium(IV) oxide has been proposed as an important approach to elimination radioactive pollution [6–12]. Heterogeneous photocatalysis with semiconductor mediated redox reactions have been proven to be effective for detoxification of harmful pollutants in waste water [13–20]. It is seen that TiO_2 shows excellent photocatalytic activity and stability [21–26], but is only active under ultraviolet light irradiation because of its wide band gap [27–29]. Therefore, many attentions are focused on the development of novel and efficient visible-light photocatalysts.

Graphitic carbon nitride (g-C_3N_4) has been widely attracted as visible-light photocatalysts for photocatalytic reduction of H_2O and CO_2 due to the high thermal and chemical stability [30–35]. The main elements of g-C_3N_4 are carbon and nitrogen. It is identified to be a visible-light-active polymeric semiconductor with a band gap of ~2.7 eV, corresponding to an optical wavelength of ~455 nm [32]. The conduction band position of pure g-C_3N_4 is at around −1.23 V (normal hydrogen electrode (NHE) at pH 7), which is more negative than the reduction potential of UO_2^{2+}/U^{4+} (0.267 V), UO_2^{2+}/UO_2 (0.411 V), and U_4O_9/UO_2 (0.456 V). Accordingly, g-C_3N_4 can be used in photocatalytic reduction of UO_2^{2+}. Although g-C_3N_4 has visible-light response, its photocatalytic activity is poor, and many attempts have been done to improve the performance, e.g., metal or non-metal element doping, and forming composites with other chemical compounds [36–38]. From the view point of application, non-metal doping is the promising strategy to improve the photocatalytic performance of pristine g-C_3N_4. For example, Yu et al have reported that sulfur doped g-C_3N_4 can enhance the photocatalytic performance in the photocatalytic reduction of CO_2 by improving the band-gap and visible-light absorption intensity

---

* Corresponding authors. Tel.: +86 791 83896550.
E-mail address: sqsong@ecit.edu.cn (S. Song).

http://dx.doi.org/10.1016/j.apsusc.2015.11.112

[39]. The study involving introducing extra electrons into g-C_3N_4 with S to transform g-C_3N_4 into superb metal-free photocatalysts for photocatalytic reduction reaction has motivated our curiosity to examine the corresponding performance of its counterpart by introducing electron-deficient element into g-C_3N_4. Intuitively, the separation of photo-generated electron and hole on the surface of the g-C_3N_4 with boron dopant (B-g-C_3N_4) should be quite easy owing to the electron-deficient property of boron, which is the precondition for the photocatalytic reduction reaction. In this study, B-g-C_3N_4 with tunable boron content of 0-1.73 at% was synthesized. The photocatalytic U (VI) reduction test indicated that B doped g-C_3N_4 showed highly efficient photocatalytic activity and stability for the reduction of U (VI). As far as we know, this is the first time for using B doped g-C_3N_4 in removing the uranium. Moreover, the origin of the photocatalytic activity of B-g-C_3N_4 including the role of the boron dopant has been discussed in detail.

2. Experimental

2.1. Photocatalysts preparation

All of the chemical reagents used in this paper were of analytic grade and were used without further purification. 10 g of thiourea was dissolved into 25 ml of H_3BO_3 aqueous solution, and then dried at 60 °C for 12 h, which can be obtained white samples. Afterwards, white powder as precursor was heated to 500 °C at a heating rate of 10 °C/min in a covered alumina crucible. The temperature was kept at 500 °C for 1.5 h and then cooled to room temperature. Then, the yellow product of B-g-C_3N_4 was obtained and ground to a fine powder. The weight ratios of precursor H_3BO_3 to g-C_3N_4 were 0, 0.5%, 1.0%, and 1.5%, and the obtained samples were labeled as g-C_3N_4, B_1-g-C_3N_4, B_2-g-C_3N_4, and B_3-g-C_3N_4, respectively.

2.2. Characterization

The X-ray diffraction (XRD) measurements were performed on a D/Max-RB X-ray diffractometer (Rigaku, Japan), utilizing Cu K_α radiation at a scanning rate (2θ) of $0.05^\circ\,s^{-1}$. The accelerating voltage and applied current were 40 kV and 80 mA, respectively. Transmission electron microscopy (TEM) analysis was carried out on a TecnaiG2 F20 S-TWIN microscope in the condition of an accelerating voltage of 200 kV. X-ray photoelectron spectroscopy (XPS) spectra were conducted by using an ultra-high-vacuum VG ESCALAB210 electron spectrometer equipped with a multichannel detector. The samples were excited using Mg K_α radiation of two anodes in the constant analyzer energy mode, and XPS was operated at 200 W. All the binding energies were referenced to the C 1speak at 284.6 eV which are adventitious carbon signals resulting from instrument or from the surface of the catalyst. Micromeritics ASAP2020 nitrogen adsorption apparatus (USA) was used to record Brunauer–Emmett–Teller (BET) specific surface area of photocatalysts and all of the samples were degassed at 180 °C before analysis. The pore size distributions were evaluated using desorption data with Barret–Joyner–Halender (BJH) method. The BET surface area was determined by a multipoint BET method to analyze the adsorption data in the relative pressure (P/P_0) range from 0.05 to 0.25. UV–vis diffuse reflection spectra (DRS) were obtained by using a dry-pressed disk sample with a UV–vis spectrophotometer (UV-2550, Shimadzu, Japan), and $BaSO_4$ is used as reflectance standard. Photoluminescence (PL) spectra were obtained on a Fluorescence Spectrophotometer (F-7000, Hitachi, Japan) at room temperature. The Photo Multiplier Tube (PMT) voltage was 700 V, the scanning speed was 1200 nm/min, and the excitation wave-length was 380 nm. The widths used for the excitation and emission slit were both 1.0 nm.

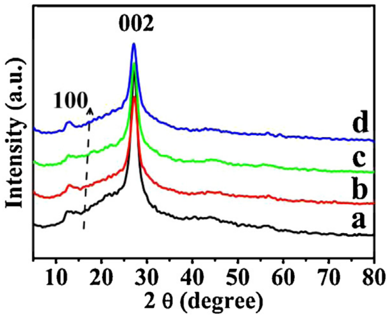

Fig. 1. XRD patterns of g-C_3N_4 and B-g-C_3N_4 samples. (a) g-C_3N_4, (b) B_1-g-C_3N_4, (c) B_2-g-C_3N_4 and (d) B_3-g-C_3N_4.

2.3. Photocatalytic tests

The photocatalytic activity tests of the prepared g-C_3N_4 samples were evaluated by the photocatalytic reduction of UO_2^{2+} solutions at ambient temperature. In the catalytic process, About 0.10 g of the as-prepared sample was added into 200 mL of 0.12 mM UO_2^{2+} solution which was prepared by dissolving uranyl nitrate ($UO_2(NO_3)_2{\cdot}6H_2O$) into mixture of deionized water and methanol. According to the calculation with visual MINTEQA using the standard thermodynamic database, hydroxide products of U (VI), e.g., $(UO_2)_3(OH)_5{}^+$ and $(UO_2)_4(OH)_7{}^+$, are the main uranium species [40], and the surface of g-C_3N_4 sample is negatively charged at pH = 7 by the Zeta potential test [41,42]. Thus, the pH of mixed suspensions was adjusted at 7.0 with diluted NaOH solution. A 500 W Xe lamp with a 420 nm cutoff filter was used as the visible light source. Before irradiation, the system was bubbled with nitrogen for 45 min to remove the air and to ensure that the reaction system is under anaerobic conditions. And then, the mixed solution was magnetically stirred in the dark for 1 h to reach the adsorption-desorption equilibrium under the anaerobic condition. After illumination for a certain time, the absorbance of UO_2^{2+} was analyzed by UVmini-1240 with using Arsenazo III Spectrophotometric Method at wavelength of 650 nm. The measured absorbance intensities at different illumination times were transformed to the reduction ratio of UO_2^{2+}, which is calculated using the following expression:

Reduction ratio of UO_2^{2+}: $\eta = C/C_0 = (A_0 - A_t)/A_0 \times 100\%$, where A_0 and A_t are the absorbance intensities when illuminated for 0 (after the dark adsorption) and t min, respectively.

3. Results and discussion

3.1. Composition and morphology of the catalysts

XRD patterns for both g-C_3N_4 and B-g-C_3N_4 samples present the consistent peaks with a well-developed g-C_3N_4 layer structure (Fig. 1). It is seen that two pronounced peaks were observed, and no obvious difference was monitored between g-C_3N_4 and B-g-C_3N_4 samples. The high-angle peak at 27.4° was characteristic of an interlayer stacking of conjugated aromatic systems, which was indexed to the (002) peak corresponding to the average interlayer distance of $d = 0.326$ nm [39,43]. A minor diffraction peak was found at low angle position of 13.1°, which was indexed to the (1 0 0) plane and assigned to the in-plane structural packing of aromatic systems with an average distance of $d = 0.675$ nm [44]. And the (1 0 0) peak shifts slightly to higher angles with increasing the content of H_3BO_3 (arrow in Fig. 1), which should be caused by the lattice contraction from the doping behavior [45,46]. The TEM images in Fig. 2 showed the morphology and microstructures of the as-prepared g-C_3N_4 and B-g-C_3N_4 samples. It is seen that all the samples show